Journal of Advanced Ceramics
2019, **8**(2): 186–195
https://doi.org/10.1007/s40145-018-0304-2
ISSN 2226-4108
CN 10-1154/TQ

Research Article

Electromechanical properties of Ce-doped $(Ba_{0.85}Ca_{0.15})(Zr_{0.1}Ti_{0.9})O_3$ lead-free piezoceramics

Raziye HAYATI[a,*], Mohammad Ali BAHREVAR[a], Yadolah GANJKHANLOU[b], Virginia ROJAS[c], Jurij KORUZA[c]

[a]*Semiconductor Division*, *Materials and Energy Research Center*, *Karaj 31787/316*, *Iran*
[b]*Department of Chemistry*, *NIS and INSTM Reference Centre*, *Università di Torino*, *Torino 10125*, *Italy*
[c]*Institute of Materials Science*, *Technische Universität Darmstadt*, *Darmstadt 64287*, *Germany*

Received: August 1, 2018; Revised: October 29, 2018; Accepted: November 8, 2018

Abstract: Lead-free piezoceramics based on the (Ba,Ca)(Zr,Ti)O_3 (BCZT) system exhibit excellent electromechanical properties for low-temperature actuation applications, but suffer from relatively high processing temperatures. Here we demonstrate an approach for the reduction of the sintering temperature and simultaneous increase of the electromechanical strain response of (Ba,Ca)(Zr,Ti)O_3 piezoceramics by aliovalent doping with Ce. The samples were prepared by solid state synthesis and their crystallographic structure, dielectric, ferroelectric, and electromechanical properties were investigated. The highest d^*_{33} value of 1189 pm/V was obtained for the sample with 0.05 mol% Ce, substituted on the A-site of the perovskite lattice. The results indicate a large potential of these materials for off-resonance piezoelectric actuators.

Keywords: lead-free piezoceramic; (Ba,Ca)(Zr,Ti)O_3 (BCZT); cerium; actuator

1 Introduction

Due to their outstanding electromechanical properties, $Pb(Zr_xTi_{1-x})O_3$ (PZT)-based ceramics were the most widely used piezoelectric materials in the past 60 years. However, the environmental and human health concerns due to the toxicity of lead forced the researchers to look for non-hazardous alternatives [1]. The most widely studied lead-free piezoceramics are based on the perovskite systems $K_{0.5}Na_{0.5}NbO_3$ (KNN) [2], $(Na_{1/2}Bi_{1/2})TiO_3$ (NBT), $BiFeO_3$ [3], and (Ba,Ca)(Zr,Ti)O_3 (BCZT) [4,5]. The solid solution of $Ba(Zr_{0.2}Ti_{0.8})O_3$–$(Ba_{0.7}Ca_{0.3})TiO_3$ was presented by Liu and Ren [6] as a pseudobinary ferroelectric system with a morphotropic phase boundary (MPB) and exceptionally-high electromechanical properties. Soon after the introduction of this new piezoelectric system in 2009, the origin of large piezoelectric coefficients became a matter of intense research and many different mechanisms were reported, among the presence of a tricritical point between cubic, tetragonal, and orthorhombic phases [7], the coexistence of tetragonal and rhombohedral phases [8], or a temperature-dependent polymorphic phase transition (PPT) with an intermediate orthorhombic phase [9]. By now, the latter seems to be widely accepted [5]. The strain mechanism in this system thus strongly depends on the chemical composition, which defines the crystallographic structure [10–12].

* Corresponding author.
E-mail: koruza@ceramics.tu-darmstadt.de

The most important material parameter for off-resonance piezoelectric actuator applications is the large signal piezoelectric coefficient ($d_{33}^{*} = S_{\text{unipolar}}^{\max} / E^{\max}$), also referred to as normalized strain. The d_{33}^{*} values reported for pure BCZT ceramics are 900–1100 pm/V (measured at 0.5 kV/mm) [6,8,13], which could be increased even further upon applying mechanical preloads [14]. Besides large strain response, BCZT compositions also exhibit a large blocking force, exceeding that of PZT based piezoceramics [15] and good fatigue resistance, i.e., cycling stability [16,17]. These properties are of high importance for the use of piezoceramics in actuating applications [18]. In addition, BCZT was recently demonstrated to promote cell viability and DNA synthesis [19], making it a promising electroactive biomaterial [20].

Despite its outstanding piezoelectric properties, the BCZT compositions suffer from a number of shortcomings, e.g., low Curie temperature (60–90 ℃), strong temperature dependence of piezoelectric properties, and high processing temperatures (1300–1500 ℃). Note that reduction of the sintering temperature, while keeping high piezoelectric properties, is highly desired from the industrial point of view [18]. In order to surmount this problem, a number of additives have been considered, among which CuO [21] and Bi_2O_3 [22] were used to densify and lower the sintering temperature of BCZT ceramics. In addition, CeO_2 has been considered for lowering the sintering temperature and improving the small signal piezoelectric coefficients of BCZT [23–25], but no comprehensive studies of large signal piezoelectric properties, which are crucial for actuator applications, were reported. Since Ce can exhibit different valence states, either 3+ or 4+, it can enter both A- and B-sites of the perovskite BCZT structure. If Ce is entering the A-site, it is expected to induce a soft piezoelectric behavior with improved piezoelectric coefficients. According to Cui *et al*. [23], small amounts of CeO_2 (< 1 mol%) reduced the sintering temperature of BCZT to 1350 ℃, without any deleterious effects on its small-signal piezoelectric properties. It should be mentioned that in the above study, CeO_2 was added to BCZT as a sintering additive, without any compensation at A- or B-sites, and the highest small signal d_{33} of 600 pC/N was obtained for BCZT sample with 0.04 wt% CeO_2. Chandrakala *et al*. [25] also studied the effects of CeO_2 on dielectric and piezoelectric properties of sol-gel synthesized BCZT. They used the same method of addition and the same amount as Cui *et al*. [23], but the samples were sintered at a higher sintering temperature (1550 ℃). They calculated the lattice strain by analyzing the X-ray diffraction (XRD) patterns and the high small signal d_{33} (670 pC/N) was attributed to a strain-induced phase transition between tetragonal and rhombohedral phases.

In this work, we investigated the influence of Ce-doping on the sintering temperature, crystallographic structure, and large signal electromechanical behavior of BCZT ceramics. The $[(Ba_{0.85}Ca_{0.15})_{1-x}Ce_{x/2}](Zr_{0.1}Ti_{0.9})O_3$ compositions with A-site compensation were sintered at 1350 ℃ and electromechanical properties were studied. Measurements of electrical properties were accompanied by Raman spectroscopy and XRD analysis. We demonstrated that the large signal d_{33}^{*} of BCZT materials can be increased by Ce-doping, while simultaneously considerably lowering the sintering temperature.

2 Materials and methods

The $[(Ba_{0.85}Ca_{0.15})_{1-x}Ce_{x/2}](Zr_{0.1}Ti_{0.9})O_3$ compositions with $0 \leqslant x \leqslant 0.05$ (abbreviated as "$BCCe_xZT$", where the subscript denotes the mol% of Ce: 0, 0.025, 0.05, 0.25, and 2.5) were synthesized via the solid-state reaction method. Raw materials of $BaCO_3$ (99.8%), $CaCO_3$ (99.5%), TiO_2 (99.6%), ZrO_2 (99.5%), and CeO_2 (99.9%) (all from Alfa-Aesar GmbH & Co. Karlsruhe, Germany) were mixed according to the stoichiometric formula and ground for 5 h at 250 rpm in ethanol using a planetary mill with zirconia balls. The calcination was done at 1300 ℃ for 3 h (heating rate 2 ℃/min). The powders were subsequently milled, dried, and uniaxially pressed into disks with a diameter of 10 mm and thickness of ~1.5 mm. Further compaction was achieved by cold isostatic pressing (CIP 100 E, Paul-Otto Weber GmbH, Remshalden, Germany) at 300 MPa. The pellets were embedded in powder of the same composition in a closed zirconia crucible and sintered in the temperature range between 1350 and 1500 ℃ for 4 h (heating rate 5 ℃/min). The sintered samples were ground to a final thickness of about 1 mm and the absolute density was measured using the Archimedes method. The theoretical density of the samples was measured on crushed and ground sintered samples by He-gas pycnometry (Micromeritics, Accu Pyc 1330, Norcross, GA, USA).

The phase composition was characterized by XRD

(D8 Advance, Bruker Inc., Germany) using Cu Kα radiation. Rietveld refinement was performed utilizing the MAUD Software. A calibration was carried out to account for the instrumental zero shift and asymmetry using the XRD pattern of Si standard sample (NBS 640). The microstructure analysis of polished samples was conducted using a field-emission scanning electron microscope (SEM; Model MIRA3 XMU, TESCAN, Czech Republic). The average grain size was calculated using the mean-intercept-length method by analyzing at least 200 grains per sample. Raman measurements were performed with a Raman spectrometer using a 633 nm radiation of an Ar^+ laser (LabRAM HR800, Horiba Scientific, Villeneuve-d′Ascq, France).

For electrical measurements, pellets were coated with silver paste and annealed at 400 ℃. Room temperature polarization and strain measurements were done using a modified Sawyer-Tower circuit and an optical displacement sensor (Model D63, Philtec Inc., Annapolis, USA), respectively. The measurements were performed with both unipolar and bipolar triangular signals with amplitude of 3 kV/mm and a frequency of 1 Hz. A commercial piezoelectric evaluation system (aix-ACCT Systems GmbH, Aachen, Germany) was used to measure the temperature dependence of polarization and strain loops. For piezoelectric measurements, poling was carried out by applying a DC electric field of 4 kV/mm to the samples at room temperature for 20 min. Temperature and frequency dependence of the dielectric permittivity were measured using an impedance analyzer equipped with a cryostat (Alpha-A, Novocontrol Technologies, Montabaur, Germany) in the frequency and temperature range of 20 Hz to 1 MHz and −100 to 150 ℃, respectively. For measuring the piezoelectric coefficients, a quasi-static d_{33}-meter was used (PM300, Piezotest Pte. Ltd., Singapore). The planar coupling factor was measured by the resonance/anti-resonance method using the same impedance analyzer described above (E = 0.1 V/mm).

3 Results and discussion

Figure 1 shows the XRD patterns of A-site Ce-substituted BCZT samples. The patterns confirm the existence of pure perovskite phase with no signs of secondary phases for all tested compositions. The undoped BCZT exhibited a combination of orthorhombic and tetragonal crystallographic structures, in agreement with previous reports [8]. For $BCCe_{2.5}ZT$, the sample with the highest Ce content, the peak splitting at 2θ = 45° is very weak and the structure is close to a cubic symmetry. Additionally, the inset in Fig. 1 shows that the peaks shift to higher 2θ angles with increasing Ce content, which indicates a contraction of the lattice after incorporation of smaller Ce ions into the A-sites (Ba^{2+}: 1.61 Å, Ca^{2+}: 1.34 Å, and Ce^{4+}: 1.14 Å). This behavior agrees well with XRD results of $(Ba_{1-x}Ce_x)TiO_3$ compositions reported elsewhere [26,27]. The modified CIF files of barium titanate with different crystal structures (cubic: 1507757, tetragonal: 1522128, and orthorhombic: 9014492) were used as a starting point for the Rietveld refinement, considering the incorporation of Ce. The refinement results are summarized in Table 1. Note that the $\chi = \sqrt{R_{wp}^2 / R_{exp}^2}$ values [28] of all refinements are below 1.8 and the difference between the measured and calculated patterns is very small (Fig. 2), indicating a good fitting.

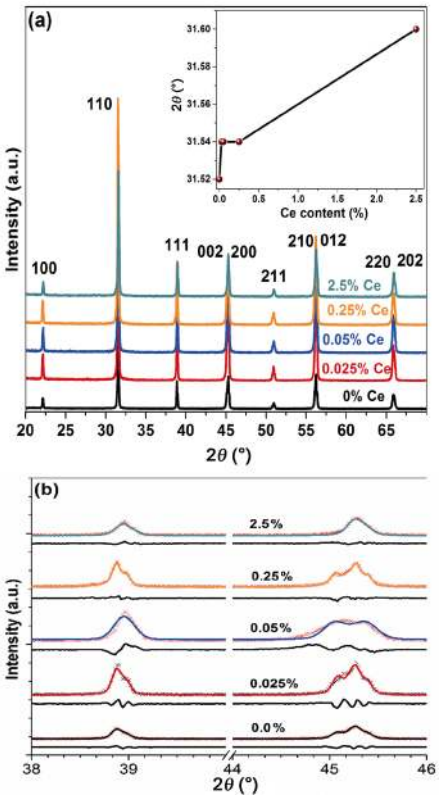

Fig. 1 (a) The XRD patterns of Ce-doped BCZT samples sintered at 1350 ℃. The numbers represent the pseudo-cubic peak labels. The inset shows the shift of the (110) peaks at 2θ = 31° with increasing the Ce content. (b) The magnification of the peaks at 2θ = 38°–40° and 44°–47°, where the symbols denote the measured values, solid colored lines the simulated pattern, and solid black lines the difference.

Table 1 Summary of the phase analysis obtained by Rietveld refinement for sintered Ce-doped BCZT samples

Ce amount (mol%)	Cubic phase (%)	Ortho-rhombic phase (%)	Tetrago-nal phase (%)	$\chi = \sqrt{R_{wp}^2 / R_{exp}^2}$	R_{wp} (%)	R_p (%)	R_{exp} (%)
0	0	86	14	1.27	15.5	11.1	12.3
0.025	0	91	9	1.76	13.5	9.3	7.7
0.05	0	96	4	1.50	11.8	8.5	8.0
0.25	11.2	75	15	1.67	12.8	8.9	7.7
2.5	88.9	10	2	1.36	12.6	9.7	9.2

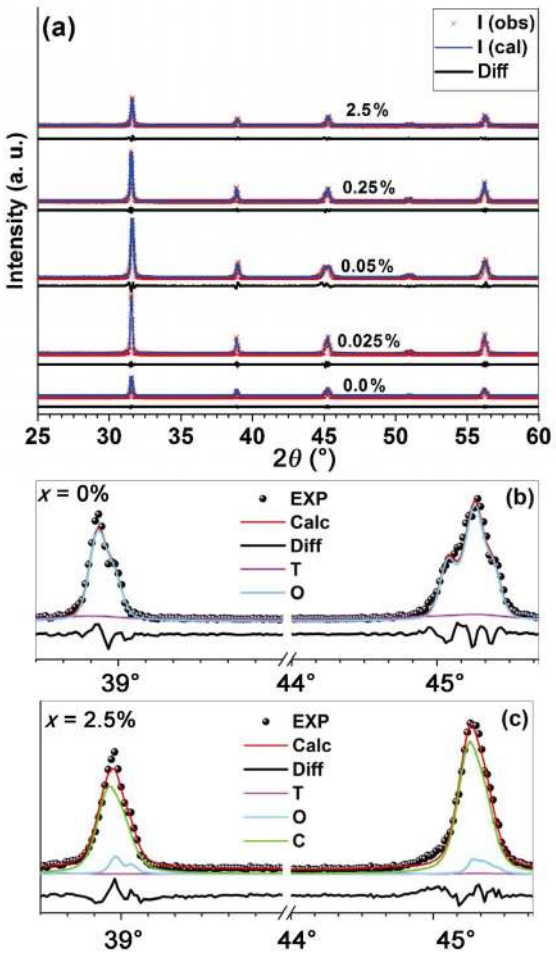

Fig. 2 (a) Rietveld refinement of the XRD patterns of $BCCe_xZT$ ceramics and the magnified peaks at $2\theta = 39°$ and 45° for (b) $x = 0$ and (c) $x = 2.5$.

The results show that by small Ce doping, the amount of the orthorhombic phase increased from 86% for pure BCZT to more than 96% for the $BCCe_{0.05}ZT$ sample. However, for Ce content higher than 0.25 mol% the crystal structure changed and a considerable amount of a non-polar cubic phase was observed in the $BCCe_{2.5}ZT$ sample, which confirms that Ce doping affects the crystal structure and lattice distortion of BCZT compositions. The changes in the phase contents are also in agreement with the observation of different vibration bands in Raman spectra, which will be discussed below.

Figure 3 shows the room temperature Raman spectra in the range of 100–1000 cm^{-1}. The Raman frequencies of tetragonal BT are at 144 (E), 177 (A_1), 195 (E), 321 (B_1), 358 (E), 447 (A_1), 527 (E), and 653 (A_1) cm^{-1} [29]. The Raman bands of BCZT are similar to those of tetragonal BT, except the presence of the A_1g mode at 811 cm^{-1} and a shift in the position of all peaks due to the incorporation of Ca^{2+} and Zr^{4+} into the BT lattice. Addition of up to 0.25 mol% Ce did not induce any considerable changes in the Raman spectra, but for higher Ce content some changes are noteworthy. The intensity of the $A_1(TO_3)$/E(TO) vibration mode ~515 cm^{-1} has decreased, which can be attributed to higher Ce incorporation into the BCZT lattice [27].

The frequency and intensity of B_1/E(TO+LO) mode at ~300 cm^{-1} decrease with increasing Ce content. This silent mode is a feature of structural changes in the lattice and its presence indicates the long-range ferroelectric order. The intensity and sharpness of the spectra have rather decreased in the $BCCe_{2.5}ZT$ sample, confirming the reduced non-cubic distortion observed in the XRD results. Accordingly, the different vibration bands in Raman spectra of the Ce-doped BCZT samples are in agreement with the changes in the phase contents of the corresponding XRD patterns. The appearance of the A_1g mode at ~840 cm^{-1} in the $BCCe_{2.5}ZT$ can indicate relaxor behavior of this sample. According to Pokorný *et al.* [30], the A_1g mode in the spectra of BT becomes Raman active upon heterovalent B-site substitution or donor substitution of A-sites. Additionally, Lu *et al.* [27] studied the Raman

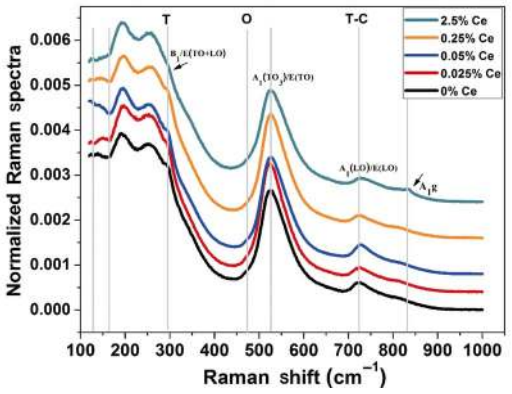

Fig. 3 Raman spectra of Ce-doped BCZT samples measured in ambient conditions.

spectra of Ce doped BT and attributed the presence of the A_1g mode to the oxygen octahedral tilting due to the substitution of Ce^{3+}/Ce^{4+} ions at Ba^{2+} sites. Curecheriu *et al*. [31] studied the relaxor behavior of the $Ba(Ce_xTi_{1-x})O_3$ composition. The absence of the A_1g mode in $BaCe_xTi_{1-x}O_3$ samples with x = 10 and 20 mol%, which was attributed to the B-site homovalent substitution, is consistent with the results of Lu *et al*. [27]. Moreover, with Ce content exceeding 10 mol%, the relaxor behavior appeared with no signs of A_1g mode. The ionic radius of A-site dopants affects the movement of oxygen atoms along the B-O-B bonds. When the difference in ionic radii is negligible, the higher atomic order in B-sites prohibits the appearance of relaxor behavior [32]. Accordingly, when there is a considerable difference between the ionic radii of the host and dopant atoms, the A_1g mode would be a good indication of the relaxor behavior. Therefore, with Ce substitution on A-sites of BCZT, it is more probable that Ce^{3+}/Ce^{4+} indeed incorporates into the Ba^{2+}/Ca^{2+} sites. However, for higher Ce contents, a part of Ce^{4+} could also enter the Ti^{4+} sites.

The SEM micrographs of polished surfaces of samples sintered at 1350 ℃ are shown in Fig. 4. The grain size increased from ~12 μm for pure BCZT to 17–18 μm for $BCCe_{0.05}ZT$ and $BCCe_{0.25}ZT$ samples and then decreased with higher Ce doping amount. Moreover, all Ce-doped samples exhibited higher densities than the undoped BCZT. According to Fig. 4(c), the $BCCe_{2.5}ZT$ sample with the highest Ce content has a relatively fine microstructure with average grain size of about 3 μm.

Figure 4(d) suggests that the influence of Ce-doping on the grain size can be divided into two regimes. For small Ce amounts (up to 0.25%), the grain size increases, which could be related to the lowering of the densification-onset temperature or to increased grain boundary mobility. The origin of this is the substitution of Ce^{3+}/Ce^{4+} ions on the Ba^{2+}/Ca^{2+} sites, as established from XRD and Raman measurements. This process induces cation vacancies, which increases the diffusion rate. Upon Ce addition above 0.25%, the grain size is drastically reduced. This value corresponds to the observed changes in the crystallographic structure (Table 1). This could be related to the proposed change of the Ce incorporation mechanism, which at this point also starts to enter the perovskite B-site. Hwang *et al*. [33] suggested that the observed grain size reduction in $(Ba_{1-x}Ce_x)TiO_3$ samples could be related to reduced formation of oxygen vacancies. However, further studies of the individual sintering stages and grain boundary mobilities are needed to elaborate these

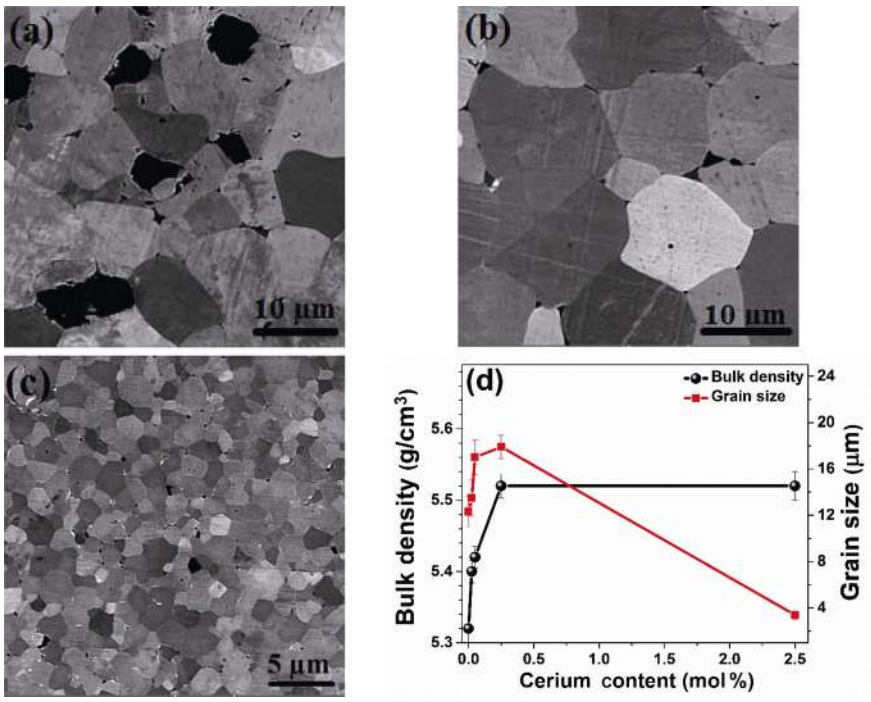

Fig. 4 SEM micrographs of polished non-etched samples with (a) 0, (b) 0.05, and (c) 2.5 mol% Ce. Micrographs were taken using backscattered electrons and orientation-contrast imaging, therefore different gray levels represent different grain orientations. (d) The influence of the Ce content on the density for the samples sintered at 1350 ℃ for 4 h.

mechanisms.

The variation of the bulk density is shown in Fig. 4(d). The density initially increased with increasing Ce content and reached a value of 5.52 g/cm^3 for $BCCe_{0.25}ZT$, which did not change for higher Ce amounts. The density increase is a result of aliovalent donor doping with Ce^{3+}/Ce^{4+} cations on the A^{2+} sites, as mentioned above. The resulting A-site vacancies promote diffusion, as previously reported in other perovskite systems [34,35]. This is in agreement with previous results for Ce-doped BT [36] and Ce-doped BCZT [37]. Issa *et al*. [38] attributed the variations in the density of Ce-doped BT to the structural changes in the lattice.

Figure 5 shows the variations of real part of dielectric permittivity and tanδ with temperature and frequency (20 Hz–1 MHz) for samples sintered at 1350 ℃. The maximum permittivity (ε_{max}) remained above 10,000 for samples with up to 0.25 mol% Ce and then decreased for higher Ce doping amounts. Besides the chemical composition, the density [39], grain/domain size [40], and lattice distortion [41] are the most important factors affecting the permittivity of polycrystalline ferroelectrics. The Ce doped samples showed higher permittivity values at room temperature, increasing from 2600 for 0 to ~8000 for 2.5 mol% Ce, whereby the latter value is the result of the induced relaxor behavior. The peaks in the dielectric curves are indicative of phase transitions and can be easily defined by the first derivatives. The following phase transitions were identified in pure BCZT: rhombohedral-orthorhombic at −2 ℃, orthorhombic-tetragonal at 27 ℃, and tetragonal-cubic (T_c) at 91 ℃. Addition of up to 0.25 mol% Ce did not influence the phase transition temperatures considerably, as the sequence of phase transition temperatures for 0.05 mol% Ce is: rhombohedral-orthorhombic at −6 ℃, orthorhombic–tetragonal at 24 ℃, and T_c at 93 ℃. A relaxor behavior and a frequency dispersion in both permittivity and loss curves were observed for the sample with 2.5 mol% Ce. This is attributed to the change in the local distortion of BO_6 octahedra that disturbs the long-range ferroelectric order [42]. The Curie temperature of pure BCZT was 91 ℃, while the temperature of the maximum permittivity for the $BCCe_{2.5}ZT$ sample was 23 ℃.

Figure 6 shows the electric field dependence of polarization (P–E) and strain (S–E) for Ce-doped BCZT samples sintered at 1350 ℃. While the P_r and P_{max} values of $BCCe_{0.025}ZT$ sample are similar to pure BCZT, further increase of Ce up to 0.25 mol% increases the maximum polarization (P_{max}), remanent polarization (P_r), and maximum strain (S_{max}). Higher Ce content led to lower polarization and narrowed hysteresis loops. However, Xiao *et al.* [43] have argued that the lower remanent polarization of BCZT with increasing Zr content may be due to three different factors, including the depression of the oriented displacement of Ti^{4+} after incorporation of Zr^{4+} and the

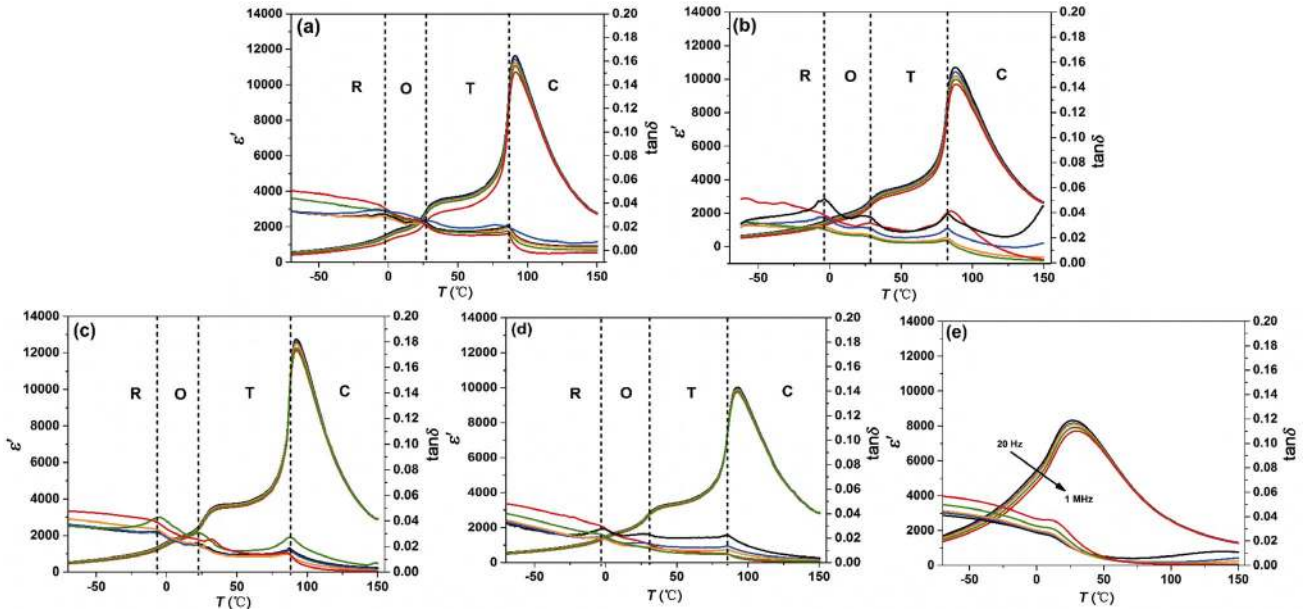

Fig. 5 Temperature-dependent real part of the dielectric permittivity and tanδ in the frequency range of 20 Hz–1 MHz, for samples sintered at 1350 ℃, with (a) 0, (b) 0.025, (c) 0.05, (d) 0.25, and (e) 2.5 mol% Ce.

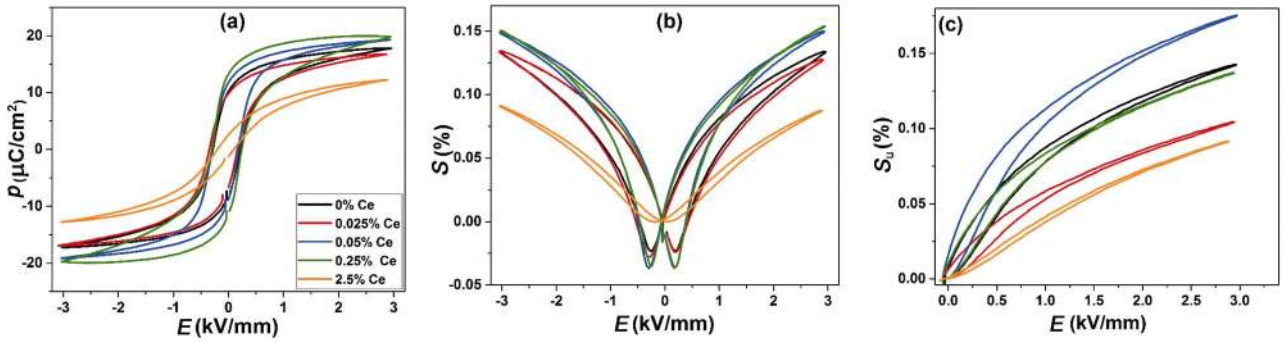

Fig. 6 (a) Bipolar polarization, (b) bipolar strain, and (c) unipolar strain loops for Ce-doped samples.

structural changes in the perovskite lattice. In the current study, the suppression of TiO_6 octahedra tilting by 2.5 mol% Ce addition may be indicated by lower P_r and E_c values in $BCCe_{2.5}ZT$ samples, which resemble relaxor behavior.

The coercive fields were determined from the maximum values of *J*–*E* loops. Ce doping led to lower E_c values, confirming the softening of piezoelectric properties. The $BCCe_{0.05}ZT$ sample had the largest value of unipolar strain, which is the more relevant parameter for actuator applications, therefore the behavior of this composition is investigated in detail below.

The variation in small and large signal piezoelectric coefficients of BCZT and $BCCe_{0.05}ZT$ samples with sintering temperature are shown in Fig. 7. The d_{33}^* values of pure BCZT increased with increasing the sintering temperature, while the $BCCe_{0.05}ZT$ samples showed a different trend. For $BCCe_{0.05}ZT$, the highest d_{33}^* of 1150 pm/V was achieved at 1350 ℃, while at the same temperature pure BCZT had a d_{33}^* of only 780 pm/V (both measured at 0.5 kV/mm). The small signal d_{33} values are shown in Fig. 7(b). The $BCCe_{0.05}ZT$ samples have higher d_{33} values than pure BCZT over the whole investigated sintering temperature range.

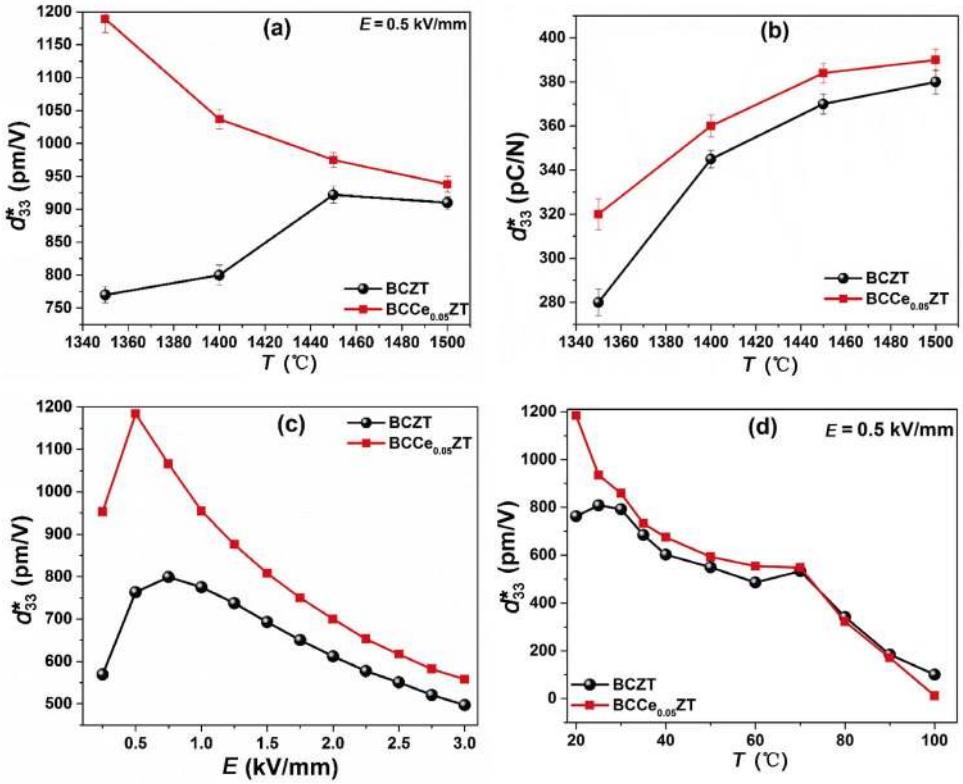

Fig. 7 Variations in piezoelectric coefficients with sintering temperature: (a) large signal d_{33}^*, (b) small signal d_{33}^*, (c) electric field dependence, and (d) temperature dependence of the large signal d_{33}^* for BCZT and $BCCe_{0.05}ZT$ samples.

Figure 7(c) compares the d^*_{33}–E plots of pure BCZT and $BCCe_{0.05}ZT$ samples, sintered at 1350 ℃. The difference between d^*_{33} values of pure and Ce-doped BCZT is large at low electric fields and decreases for higher electric fields. This indicates that Ce-doped samples can be efficiently driven at lower electric fields, which is an important property for actuation applications and enables further device miniaturization. The temperature dependence of d^*_{33} is shown in Fig. 7(d). As it is seen, the trend has not changed after Ce doping and by approaching the O–T and T–C transition temperatures, the values of d^*_{33} increased. The d^*_{33} values of $BCCe_{0.05}ZT$ sample are higher than those of pure BCZT up to 70 ℃.

A summary of dielectric, ferroelectric, and piezoelectric properties of Ce-doped BCZT samples is shown in Table 2. Ce addition improved the electrical properties up to 0.25 mol%, but the ferroelectric behavior changed to diffuse and relaxor-like behavior in the $BCCe_{2.5}ZT$ sample. The Curie temperature remained unaltered up to 0.25 mol% Ce. Upon addition of 0.05 mol% Ce, polarization, strain improved, and large d^*_{33} values were obtained.

The pseudocubic structure (Figs. 1 and 2), appearance of the A_1g mode (Fig. 3), the dispersion in the dielectric permittivity (Fig. 5(e)), and the slim polarization/strain hysteresis loops (Fig. 6), indicate the relaxor nature of the $BCCe_{2.5}ZT$ sample. This is confirmed by the strain vs. polarization square plot in Fig. 8, whereby a linear relationship is observed. The reasonable linear fit confirms the nearly hysteresis-free electrostrictive behavior of this sample, whereby the slope can be related to the electrostrictive coefficient Q_{33} [44]. A relatively high, temperature independent value of 0.063 m^4/C^2 was obtained for $BCCe_{2.5}ZT$ sample, as it is shown in Fig. 8(b).

4 Conclusions

Substitution of BCZT A-site ions with Ce is demonstrated to be an efficient approach to enhance densification and improve the electromechanical properties of this lead-free piezoelectric material. The incorporation of Ce on A-sites was confirmed by structural studies. The highest d^*_{33} value of 1189 pm/V was obtained for the sample with 0.05 mol% Ce sintered at 1350 ℃, which is approximately 100–150 ℃ lower compared

Table 2 Summary of room temperature electrical properties of Ce-doped BCZT samples sintered at 1350 ℃

Ce amount (mol%)	T_C (℃)	ε @ RT, 1 kHz	tanδ	P_r (μC/cm^2)	E_C (kV/mm)	S_{max} (%) @ 0.5 kV/mm	d^*_{33} (pm/V) @ 0.5 kV/mm
0	91	2617	0.044	9.6	0.27	0.042	763
0.025	89	2495	0.037	10.0	0.38	0.027	541
0.05	93	2730	0.029	11.6	0.24	0.060	1189
0.25	93	2363	0.032	13.0	0.27	0.044	870
2.5	23	8297	0.014	2.5	0.15	0.016	326

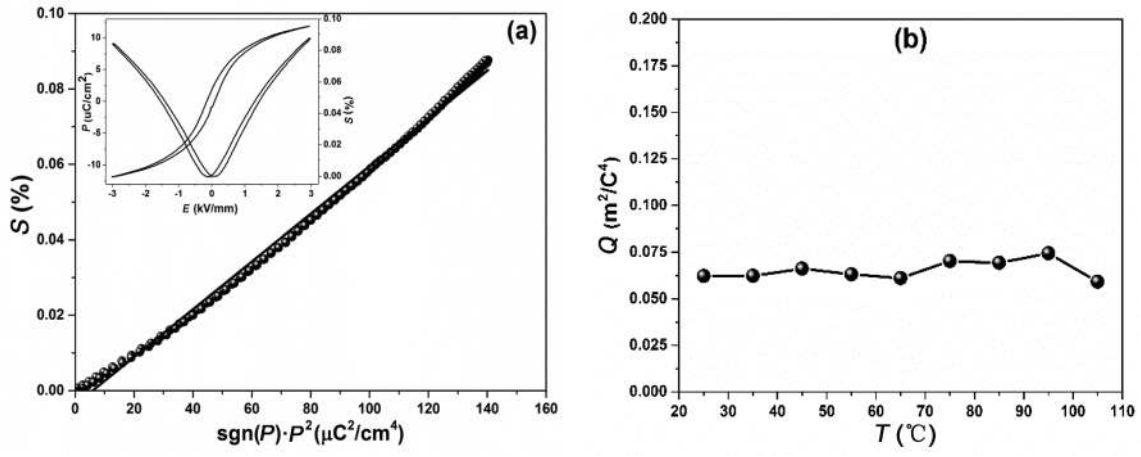

Fig. 8 (a) The plot of strain vs. square polarization and (b) the temperature dependence of bipolar electrostrictive coefficient Q_{33} for $BCCe_{2.5}ZT$ sample.

to typical sintering temperatures of pure BCZT. The high room-temperature values were related to the proximity of the O-T phase transition and enhanced reversible extrinsic strain contributions. Higher doping amounts (2.5 mol% Ce) resulted in a reduction of the grain size and relaxor properties of the sample, evidenced by frequency dispersion of the temperature-dependent permittivity, slim polarization, strain hysteresis loops, and a high electrostrictive coefficient.

Acknowledgements

This work was funded by Ministry of Science, Research and Technology of Iran as a Ph.D. project, with Grant No. 481392053, at Materials & Energy Research Center (MERC). It was also partially supported by Deutsche Forschungsgemeinschaft under the Sonderforschungsbereich 595 (SFB 595) fellowship.

References

[1] Rödel, J, Jo W, Seifert KTP, *et al*. Perspective on the development of lead-free piezoceramics. *J Am Ceram Soc* 2009, **92**: 1153–1177.

[2] Safari A, Hejazi M. Lead-free KNN-based piezoelectric materials. In *Lead-free Piezoelectrics*. Priya S, Nahm S, Eds. New York: Springer, 2012: 139–175.

[3] Nagata H, Takenaka T. Chapter 4-Bi-based lead-free piezoelectric ceramics. In *Advanced Piezoelectric Materials*. 2nd edn. Sawston, Cambridge: Woodhead Publishing, 2017: 155–196.

[4] Zhang Y, Sun HJ, Chen W. A brief review of $Ba(Ti_{0.8}Zr_{0.2})O_3$–$(Ba_{0.7}Ca_{0.3})TiO_3$ based lead-free piezoelectric ceramics: past, present and future perspectives. *J Phys Chem Solids* 2017, **114**: 207–219.

[5] Acosta M, Novak N, Rojas V, *et al*. $BaTiO_3$-based piezoelectrics: fundamentals, current status, and perspectives. *Appl Phys Rev* 2017, **4**: 041305.

[6] Liu WF, Ren XB. Large piezoelectric effect in Pb-free ceramics. *Phys Rev Lett* 2009, **103**: 257602.

[7] Benabdallah F, Simon A, Khemakhem H, *et al*. Linking large piezoelectric coefficients to highly flexible polarization of lead free $BaTiO_3$-$CaTiO_3$-$BaZrO_3$ ceramics. *J Appl Phys* 2011, **109**: 124116.

[8] Ehmke MC, Ehrlich SN, Blendell JE, *et al*. Phase coexistence and ferroelastic texture in high strain $(1-x)Ba(Zr_{0.2}Ti_{0.8})O_3$–$x(Ba_{0.7}Ca_{0.3})TiO_3$ piezoceramics. *J Appl Phys* 2012, **111**: 124110.

[9] Keeble DS, Benabdallah F, Thomas PA, *et al*. Revised structural phase diagram of $(Ba_{0.7}Ca_{0.3}TiO_3)$-$(BaZr_{0.2}Ti_{0.8}O_3)$. *Appl Phys Lett* 2013, **102**: 092903.

[10] Acosta M, Novak N, Rossetti GA, *et al*. Mechanisms of electromechanical response in $(1-x)Ba(Zr_{0.2}Ti_{0.8})O_3$–$x(Ba_{0.7}Ca_{0.3})TiO_3$ ceramics. *Appl Phys Lett* 2015, **107**: 142906.

[11] Acosta M, Novak N, Wook J, *et al*. Relationship between electromechanical properties and phase diagram in the $Ba(Zr_{0.2}Ti_{0.8})O_3$–$x(Ba_{0.7}Ca_{0.3})TiO_3$ lead-free piezoceramic. *Acta Mater* 2014, **80**: 48–55.

[12] Gao JH, Hu XH, Zhang L, *et al*. Major contributor to the large piezoelectric response in $(1-x)Ba(Zr_{0.2}Ti_{0.8})O_3$ – $x(Ba_{0.7}Ca_{0.3})TiO_3$ ceramics: Domain wall motion. *Appl Phys Lett* 2014, **104**: 252909.

[13] Hao JG, Bai WF, Li W, *et al*. Correlation between the microstructure and electrical properties in high-performance $(Ba_{0.85}Ca_{0.15})(Zr_{0.1}Ti_{0.9})O_3$ lead-free piezoelectric ceramics. *J Am Ceram Soc* 2012, **95**: 1998–2006.

[14] Ehmke MC, Schader FH, Webber KG, *et al*. Stress, temperature and electric field effects in the lead-free $(Ba,Ca)(Ti,Zr)O_3$ piezoelectric system. *Acta Mater* 2014, **78**: 37–45.

[15] Brandt DRJ, Acosta M, Koruza J, *et al*. Mechanical constitutive behavior and exceptional blocking force of lead-free BZT-*x*BCT piezoceramics. *J Appl Phys* 2014, **115**: 204107.

[16] Zhang Y, Glaum J, Ehmke MC, *et al*. High bipolar fatigue resistance of BCTZ lead-free piezoelectric ceramics. *J Am Ceram Soc* 2016, **99**: 174–182.

[17] Rojas V, Koruza J, Patterson EA, *et al*. Influence of composition on the unipolar electric fatigue of $Ba(Zr_{0.2}Ti_{0.8})O_3$–$(Ba_{0.7}Ca_{0.3})TiO_3$ lead-free piezoceramics. *J Am Ceram Soc* 2017, **100**: 4699–4709.

[18] Koruza J, Bell AJ, Frömling T, *et al*. Requirements for the transfer of lead-free piezoceramics into application. *Journal of Materiomics*, 2018, **4**: 13–26.

[19] Acosta M, Detsch R, Grünewald A, *et al*. Cytotoxicity, chemical stability, and surface properties of ferroelectric ceramics for biomaterials. *J Am Ceram Soc* 2018, **101**: 440–449.

[20] Yap EW, Glaum J, Oddershede J, *et al*. Effect of porosity on the ferroelectric and piezoelectric properties of $(Ba_{0.85}Ca_{0.15})(Zr_{0.1}Ti_{0.9})O_3$ piezoelectric ceramics. *Scripta Mater* 2018, **145**: 122–125.

[21] Chen T, Zhang T, Wang G, *et al*. Effect of CuO on the microstructure and electrical properties of $Ba_{0.85}Ca_{0.15}Ti_{0.90}Zr_{0.10}O_3$ piezoceramics. *J Mater Sci* 2012, **47**: 4612–4619.

[22] Hayati R, Bahrevar M, Ebadzadeh T, *et al*. Effects of Bi_2O_3 additive on sintering process and dielectric, ferroelectric, and piezoelectric properties of $(Ba_{0.85}Ca_{0.15})(Zr_{0.1}Ti_{0.9})O_3$ lead-free piezoceramics. *J Eur Ceram Soc* 2016, **36**: 3391–3400.

[23] Cui YR, Liu XY, Jiang MH, *et al*. Lead-free $(Ba_{0.85}Ca_{0.15})(Ti_{0.9}Zr_{0.1})O_3$–$CeO_2$ ceramics with high piezoelectric coefficient

obtained by low-temperature sintering. *Ceram Int* 2012, **38**: 4761–4764.

[24] Chandrakala E, Praveen JP, Kumar A, *et al*. Strain-induced structural phase transition and its effect on piezoelectric properties of (BZT-BCT)-(CeO_2) ceramics. *J Am Ceram Soc* 2016, **99**: 3659–3669.

[25] Chandrakala E, Praveen JP, Das D. Effect of poling process on piezoelectric properties of BCZT–0.08 wt.% CeO_2 lead-free ceramics. *AIP Conf Proc* 2016, **1728**: 020502.

[26] Hwang JH, Han YH. Electrical properties of cerium-doped $BaTiO_3$. *J Am Ceram Soc 2001*, **84**: 1750–1754.

[27] Lu DY, Han DD, Sun XY, *et al*. Raman evidence for Ba-site Ce^{3+} in $BaTiO_3$. *Jpn J Appl Phys* 2013, **52**: 111501.

[28] Toby BH. R Factors in Rietveld analysis: How good is good enough. *Power Diffra* 2006, **21**: 67–70.

[29] Seo YS, Ahn JS, Jeong IK. Soft modes and local structural transitions in Pb-free $Ba(Ti_{0.8}Zr_{0.2})O_3$-$x(Ba_{0.7}Ca_{0.3})TiO_3$ (x=0.5): pressure- and temperature- dependent Raman studies. *J Korean Phys Soc* 2013, **62**: 749–755.

[30] Pokorný J, Pasha UM, Ben L, *et al*. Use of Raman spectroscopy to determine the site occupancy of dopants in $BaTiO_3$. *J Appl Phys* 2011, **109**: 114110.

[31] Curecheriu LP, Deluca M, Mocanu ZV, *et al*. Investigation of the ferroelectric–relaxor crossover in Ce-doped $BaTiO_3$ ceramics by impedance spectroscopy and Raman study. *Phase Transit* 2013, **86**: 703–714.

[32] Ganguly M, Rout SK, Sinha TP, *et al*. Characterization and Rietveld refinement of A-site deficient lanthanum doped barium titanate. *J Alloys Compd* 2013, **579**: 473–484.

[33] Hwang JH, Han YH. Electrical properties of cerium-doped $BaTiO_3$. *J Am Ceram Soc* 2001, **84**: 1750–1754.

[34] Malič B, Koruza J, Hreščak J, *et al*. Sintering of lead-free piezoelectric sodium potassium niobate ceramics. *Materials* 2015, **8**: 8117–8146.

[35] Bernard J. *Piezoelectric Ceramics*. London and New York (England and USA): Academic Press, 1971.

[36] Han F, Bai Y, Qiao LJ, *et al*. A systematic modification of the large electrocaloric effect within a broad temperature range in rare-earth doped $BaTiO_3$ ceramics. *J Mater Chem C* 2016, **4**: 1842–1849.

[37] Chandrakala E, Praveen PJ, Kumar A, *et al*. Strain-induced structural phase transition and its effect on piezoelectric properties of (BZT-BCT)-(CeO_2) ceramics. *J Am Ceram Soc* 2016, **99**: 3659–3669.

[38] Issa MAA, Molokhia NM, Dughaish ZH. Effect of cerium oxide (CeO_2) additives on the dielectric properties of $BaTiO_3$ ceramics. *J Phys D: Appl Phys* 1983, **16**: 1109.

[39] Dube DC. Study of Landau-Lifshitz-Looyenga's formula for dielectric correlation between powder and bulk. *J Phys D: Appl Phys* 1970, **3**: 1648.

[40] Arlt G, Hennings D, de With G. Dielectric properties of fine-grained barium titanate ceramics. *J Appl Phys* 1985, **58**: 1619–1625.

[41] Kolodiazhnyi T, Petric A. Analysis of point defects in polycrystalline $BaTiO_3$ by electron paramagnetic resonance. *J Phys Chem Solids* 2003, **64**: 953–960.

[42] Canu G, Confalonieri G, Deluca M, *et al*. Structure-property correlations and origin of relaxor behaviour in $BaCe_xTi_{1-x}O_3$. *Acta Mater* 2018, **152**: 258–268.

[43] Xiao F, Ma WB, Sun QC, *et al*. The electrostrictive effect and dielectric properties of lead-free $0.5Ba(Zr_xTi_{1-x})O_3$–$0.5(Ba_{0.75}Ca_{0.25})TiO_3$ ceramics. *J Mater Sci: Mater Electron* 2013, **24**: 2653–2658.

[44] Li F, Jin L, Xu Z, *et al*. Electrostrictive effect in ferroelectrics: An alternative approach to improve piezoelectricity. *Appl Phys Rev* 2014, **1**: 011103.